



Photocatalytic degradation of methylene blue from aqueous solution using $\text{Fe}_3\text{O}_4@\text{SiO}_2@\text{CeO}_2$ core-shell magnetic nanostructure as an effective catalyst

Fatemeh Ziaadini^a, Ali Mostafavi^a, Tayebeh Shamspur^a, Fariba Fathirad^{b*}

^aDepartment of Chemistry, Faculty of Science, Shahid Bahonar University of Kerman, Kerman, Iran

^bDepartment of Nanotechnology, Graduate University of Advanced Technology, Kerman, Iran

ARTICLE INFO

Article history:

Received 25 March 2020

Received in revised form

19 April 2020

Accepted 29 May 2020

Keywords:

Core-shell magnetic nanostructure
Photo degradation
Visible light driven
Methylene blue

ABSTRACT

In the present study, the core-shell magnetic nanostructure of $\text{Fe}_3\text{O}_4@\text{SiO}_2@\text{CeO}_2$ was synthesized to investigate its use as an effective photocatalyst for methylene blue removal. The prepared samples were characterized by X-ray diffraction (XRD), transmission electron microscopy (TEM), and a vibrating sample magnetometer (VSM). The photocatalytic activity for the $\text{Fe}_3\text{O}_4@\text{SiO}_2@\text{CeO}_2$ core-shell magnetic nanostructure was investigated under visible light by determining the degradation rate of methylene blue for 50 min. At the end of the photocatalytic degradation process, the magnetic catalyst was recovered by an external magnetic field. The performance of the proposed catalyst for the degradation of methylene blue was improved with the optimization of the effective parameters such as the amount of catalyst, pH, and reaction time. Under optimum conditions, the efficiency of methylene blue removal with the proposed photocatalyst remains higher than 92 % after five times of use. The second pseudo-model was selected as the kinetic model to calculate catalytic degradation. The present results show that the $\text{Fe}_3\text{O}_4@\text{SiO}_2@\text{CeO}_2$ can be an efficient nanocatalyst for the photodegradation of dye pollutants.

1. Introduction

Photocatalysts are activated in the presence of light. They are usually semiconducting solid oxides, which create a pair of electron-cavity by absorbing the photons. This electron-cavity can react with molecules in the surface of the particles, and directly or indirectly produce radical hydroxyls that convert organic matter into minerals [1-2]. Photocatalysts are used in water purification, air purification, self-cleaning glasses, anti-steam surfaces, antimicrobials, and organic molecules [3]. Nanostructured materials have physical-chemical properties due to their small size that increases surface-to-volume ratio [4-5]. Nanotechnology is widely used in various industries including textile, electronic, construction, biomedical, pharmaceutical, etc. [6-8]. Some nanoparticles are used as photocatalysts: TiO_2 , ZnO , Fe_2O_3 , WO_3 and CeO_2 [9-10]. Cerium dioxide has been studied for its use in photocatalytic

applications for the treatment of organic pollutant because of its high surface-to-volume ratio, photosensitivity, photochemical stability, and non-toxicity [11]. The Core-shell type nanostructure consists of a core (inner material) and a shell (outer layer material). Each core and shell have properties such as metal conductivity, semiconductivity, magnetism, etc. Core-shell nanostructures are important from an economic point of view because the surface of valuable materials can be covered by a cheap material, which reduces its consumption [12]. The coating on the core can increase surface area, improve surface properties, increase performance, and reduce the cost of consuming expensive materials [13]. Creating an appropriate organic or inorganic coating on the surface of the magnetic core increases the lifespan of these particles [14]. Core-shell magnetic nanostructures have a greater capacity to remove organic pollutants from wastewater. Also, magnetic

*Corresponding author.

E-mail address: f_fathirad@yahoo.com

DOI:10.22104/AET.2020.4137.1204

nanoparticles are absorbed using a magnetic field, which helps to extract the sample in the chemical analysis [15-17]. Methylene blue (MB) is one of the synthetic dyes with a molecular formula of $C_{16}H_{18}N_3SCl$. The concentration of 2-4 ppm of MB causes anemia and skin problems in infants, 7 ppm causes nausea and chest pain, 20 ppm causes blood pressure, and 80 ppm turns the skin blue [18-19]. The semiconductor properties of the photocatalyst reduces pollutants such as MB. The core-shell nanostructures have a high adsorption capacity, photocatalytic properties, and the ability to regenerate. They have attracted much attention in the field of sustainable development and the improvement of environmental issues [20-21]. The purpose of this study was the synthesis of Fe_3O_4 , $Fe_3O_4@SiO_2$, CeO_2 , and $Fe_3O_4@SiO_2@CeO_2$ core-shell magnetic nanostructure and a comparison of their abilities as a photocatalyst for the removal of methylene blue under visible light. After selecting the most promising photocatalyst, the effect of the other variables influencing the process was investigated.

2. Materials and methods

2.1. Chemicals

The $FeSO_4 \cdot 7H_2O$, $FeCl_3 \cdot 6H_2O$, ethylene glycol, and polyethylene glycol were purchased from Merck. The tetraethyl orthosilicate (TEOS), $Ce(SO_4)_2 \cdot 4H_2O$, and methylene blue were purchased from Sigma-Aldrich.

2.2. Preparation of Fe_3O_4 magnetic core

The iron oxide magnetic nanoparticles (MNPs) were synthesized through the coprecipitation method. Iron (III) chloride hexahydrate (3.1 g, 10 mmol) and iron (II) sulfate hexahydrate (1.6 g, 5 mmol) were dissolved in distilled water (130 mL) under N_2 atmosphere. Then, ammonium hydroxide 20 % was slowly added to the solution, while the pH value was controlled in the range of 8-9. The precipitate was collected using a magnet and washed several times with distilled water and ethanol until reaching a neutral pH; it was dried at 70 °C for 12 h.

2.3. Preparation of $Fe_3O_4@SiO_2$ magnetic core

The $Fe_3O_4@SiO_2$ nanoparticles were synthesized through the Stöber method. The 200 mL ethanol solution containing 1g Fe_3O_4 powder was ultrasound for 30 min. Then, 5 mL of ammonia was added to the solution. Subsequently, 1 mL of TEOS diluted in ethanol (20 mL) was added dropwise, and the resulting mixture was stirred for 24 hours at room temperature. The magnetic $Fe_3O_4@SiO_2$ nanoparticles were collected by a magnet and washed with distilled water and ethanol, and dried at room temperature for 48 h.

2.4. Preparation of $Fe_3O_4@SiO_2@CeO_2$ magnetic core-shell

The $Fe_3O_4@SiO_2@CeO_2$ nanostructure was synthesized by homogeneous precipitation and subsequently calcinated. The 0.5 g of $Fe_3O_4@SiO_2$ in 50 mL ethylene glycol was stirred under ultrasound waves for 50 min at 50 °C. The 10 mL aqueous solution containing 10 mM cerium sulfate tetrahydrate was added dropwise to the first solution. It was stirred in the same state for 30 min. Subsequently, 25 mL of 3 M ammonia was added, and the solution was stirred at 50 °C for 12 h. The precipitate was separated by a magnet and dried at 80 °C for 24 h in an oven. Finally, the magnetic nanostructure was calcinated at 500 °C for 2 h.

2.5. Photocatalytic degradation of dye

The photocatalytic activity of the prepared nanostructure was assessed by monitoring the degradation of methylene blue in an aqueous solution under the visible light irradiation. 0.05 g of nanocatalyst was added to 20 mL of 10 ppm MB solution at a pH = 11. The suspension was stirred using a magnetic stirrer for 50 min under visible light. The degradation efficiency of MB by the nanocatalyst was evaluated by a UV-Vis spectrophotometer, and the percent of dye removal was calculated using the following equation: $Removal (\%) = (C_0 - C) / C_0 \times 100$ where C_0 and C represent the concentration of MB at the initial and final condition, respectively.

3. Results and discussion

3.1. Characterization of photocatalyst

The product X-ray diffraction (XRD) data were recorded by a Rigaku D-max C III- X-ray diffractometer using Ni-filtered $Cu_{K\alpha}$ radiation. The composition of the photocatalyst was characterized by a transmitting electron microscope (TEM), model LEO-912 AB, manufactured in Germany. The magnetic properties were examined using a vibrating sample magnetometer (VSM) at room temperature. All absorption measurements were carried out with an ultraviolet Specord 210 plus spectrophotometer produced by the Analytikjena Company, Germany. The XRD patterns of the Fe_3O_4 , $Fe_3O_4@SiO_2$ and $Fe_3O_4@SiO_2@CeO_2$ magnetic core-shell are shown in Figure 1. The peaks of the Fe_3O_4 nanoparticles at the scattering angles (2θ) of 30.3°, 36°, 43.3°, 54°, 57°, 63°, and 74° were related to the diffraction plates of (220), (311), (400), (422), (511), (440), and (533), respectively. The coating of the magnetic nanoparticles of iron oxide with the amorphous silica phase did not differ in the XRD pattern. The successful coating of the $Fe_3O_4@SiO_2$ core-shell with CeO_2 shell was confirmed with the presence of the new phase regarding CeO_2 . The peaks of the CeO_2 nanoparticles at scattering angles (2θ) of 28.74°, 33.28°, 47.61°, 56.53°, 69.61°, and 76.83° were related to the diffraction plates of (111), (200), (220), (311), (222), and (400), respectively.

The $\text{Fe}_3\text{O}_4@\text{SiO}_2@\text{CeO}_2$ nanostructure was characterized by TEM. Figure 2 shows that this photocatalyst has a core-shell structure, including a magnetic Fe_3O_4 core, a SiO_2 middle layer, and a CeO_2 particle coating [22]. According to the image, the size of the nanoparticles is about 40 nm. The magnetic properties of the nanostructures were examined at room temperature using VSM. Figure 3 shows that the Ms values of $\text{Fe}_3\text{O}_4@\text{SiO}_2$ and $\text{Fe}_3\text{O}_4@\text{SiO}_2@\text{CeO}_2$ were lower than that of the Fe_3O_4 because the Fe_3O_4 magnetic core was subsequently coated with a layer of SiO_2 and CeO_2 , which led to a decrease in magnetism.

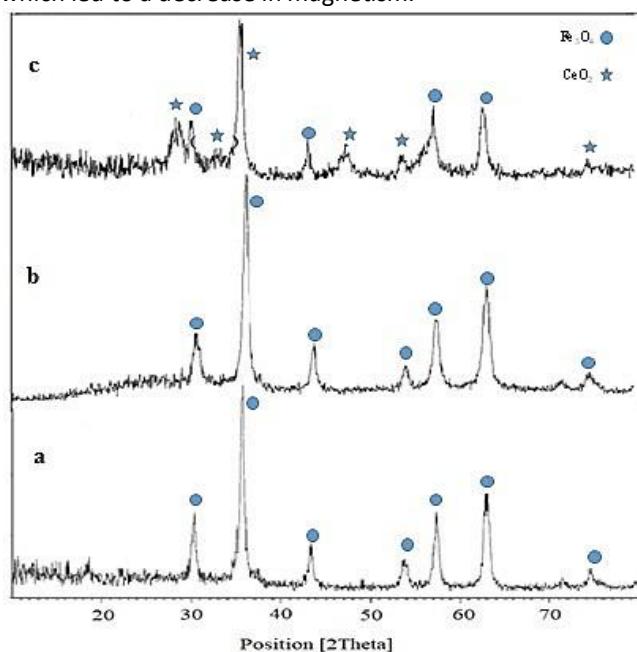


Fig. 1. The XRD patterns of a) Fe_3O_4 , b) $\text{Fe}_3\text{O}_4@\text{SiO}_2$, and c) $\text{Fe}_3\text{O}_4@\text{SiO}_2@\text{CeO}_2$ nanoparticles.

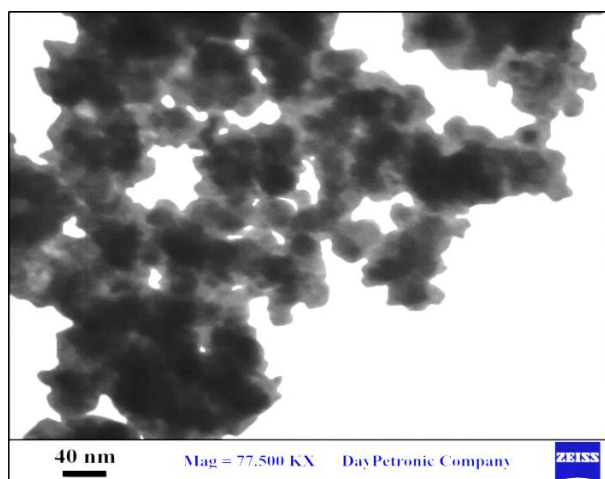


Fig. 2. TEM image of $\text{Fe}_3\text{O}_4@\text{SiO}_2@\text{CeO}_2$ nanoparticles.

3.2. Comparison of Photocatalytic Performance of Synthesized Nanostructures

The photocatalytic performance of different nanostructures in MB degradation was investigated according to the procedure in section 2.5. Figure 4 shows the recorded UV-

Vis spectra from the solutions after being exposed to the visible light. Figure 4(a) shows the spectrum of the solution without photocatalysis performance. Figure 4b and c shows the previous solution after the performance of Fe_3O_4 and $\text{Fe}_3\text{O}_4@\text{SiO}_2$ in the presence of visible light. As shown, these nanostructures have no photocatalytic activity. As shown in Figure 4d, the $\text{Fe}_3\text{O}_4@\text{SiO}_2@\text{CeO}_2$ core-shell magnetic nanostructure has a good photocatalytic performance in the degradation of MB dye under visible light. This photoactivity is ascribed to the ceria photocatalytic properties that improve due to the surface properties of magnetic catalyst. These surface properties provides more surface active sites for the adsorption of organic molecules, causing higher efficiency in photocatalytic activity [22]. According to this, $\text{Fe}_3\text{O}_4@\text{SiO}_2@\text{CeO}_2$ was selected as the best photocatalyst. In the following section, the effective parameters on the dye removal in the presence of this catalyst were investigated and optimized.

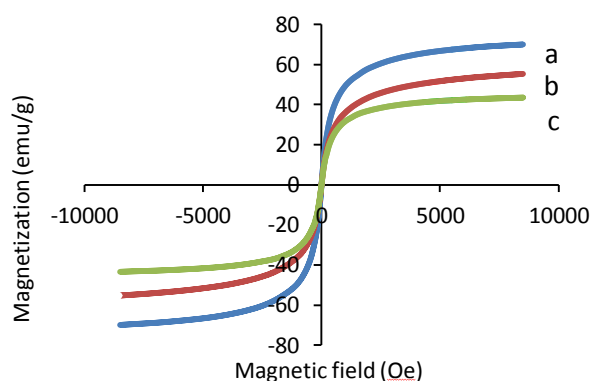


Fig. 3. Hysteresis loops of (a) Fe_3O_4 , (b) $\text{Fe}_3\text{O}_4@\text{SiO}_2$, and (c) $\text{Fe}_3\text{O}_4@\text{SiO}_2@\text{CeO}_2$.

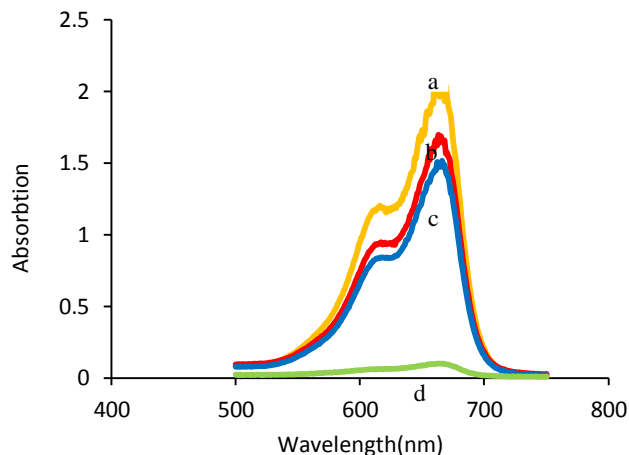


Fig. 4. UV-Vis spectra of MB solution (a) before and after (b) Fe_3O_4 , (c) $\text{Fe}_3\text{O}_4@\text{SiO}_2$, and (d) $\text{Fe}_3\text{O}_4@\text{SiO}_2@\text{CeO}_2$ nanoparticles photocatalytic performance.

3.3. Effect of different parameters on the photocatalytic removal of MB dye

The dye removal efficiency was carried out under varying pH from 6 to 11, which were adjusted with HCl and NaOH.

With increasing pH, the number of sites with negative charge increased due to the presence of hydroxyl ions. As a result, electrostatic gravity was generated between the photocatalyst and the cation dye, and the MB removal efficiency increased at the aqueous solution. As shown in Figure 5, the highest percentage of removal occurred in a pH = 11, which was selected as the optimum pH. The amount of photocatalyst varied from 0.005 to 0.2 g, and the experiments were continued. The increasing amounts made the reaction faster due to an increase in the number of active sites on the photocatalyst. A further increase in the amount of photocatalyst above 0.05 g had a negligible effect on the MB removal efficiency, which could be due to the hindrance to the pathway of light to reach the dye molecules. The optimum value for the photocatalyst was 0.05 g. To evaluate the effect of the irradiation time on the MB removal efficiency, the solutions were exposed to visible light for 10 to 100 min. In the beginning, due to the presence of high amounts of MB in the solution, the binding rate to the sites was high, and the removal efficiency increased but stabilized after 50 minutes. Therefore, the reaction time of 50 min was selected. The effect of initial dye level on the removal efficiency was studied by investigating different concentrations between 5 to 30 ppm. According to Figure 6, the photocatalytic process was more effective at a concentration of 10 ppm.

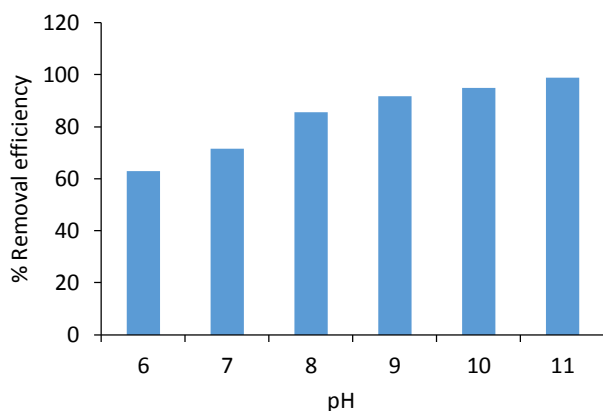


Fig. 5. Effect of pH on photocatalytic activity and removal of methylene blue dye.

3.4. Stability and Reuse Investigation

Sustainability and reuse of the core-shell magnetic nanostructure as the photocatalyst in methylene blue degradation was investigated under optimum condition. The percentage of methylene blue removal with the photocatalyst remains more than 92% after five times of use (Figure 7). This means that the proposed photocatalyst can be reused for at least five times without losing a significant amount of its performance and has good stability.

3.5. Investigation of Photocatalytic Degradation Kinetics

Equation (1) is a first-pseudo kinetic model equation in which q_e is the removed dye when stabilized (mg/g), q_t is the

removed dye at t time (mg/g), and K_1 is the speed constant of the first -pseudo order (min^{-1}).

$$\log(q_e - q_t) = \log q_e - \frac{K_1 t}{2.303} \quad (1)$$

$$\frac{t}{q_t} = \frac{1}{q_e^2 K_2} + \frac{t}{q_e} \quad (2)$$

Equation (2) is a second -pseudo kinetic model equation in which k_2 is the speed constant of the second-pseudo order (min^{-1}).

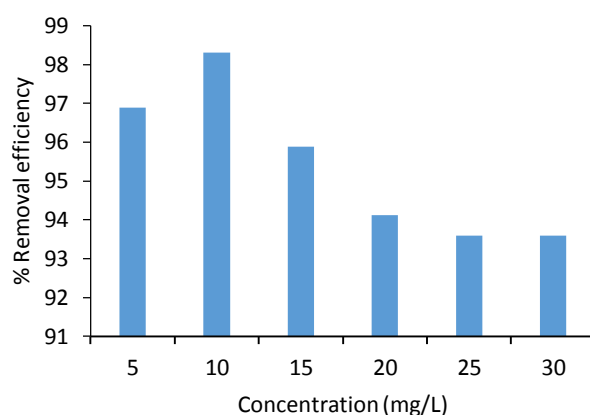


Fig. 6. Effect of solution concentration on methylene blue removal efficiency.

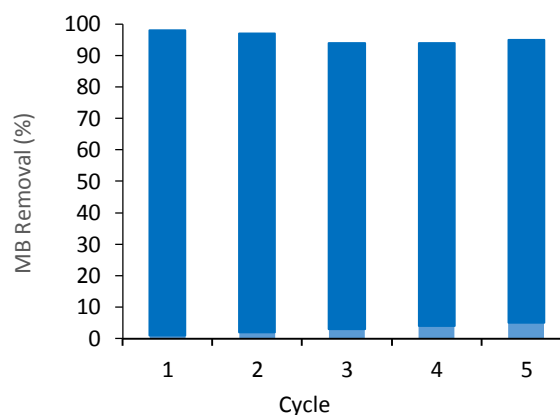


Fig. 7. Investigation of photocatalyst reusability in the methylene blue removal.

In Figure 8, the parameters of the first-pseudo and second-pseudo kinetic model are presented. According to the results, the photocatalytic degradation of MB in the presence of the proposed photocatalyst is based on the second pseudo-model.

3.6. Comparison of proposed nanostructures with other photocatalysts

In Table 1, the proposed photocatalyst is compared with other photocatalysts [23-27] for MB degradation. The $\text{Fe}_3\text{O}_4@\text{SiO}_2@\text{CeO}_2$ nanostructure can remove more MB with less photocatalyst consumption in a shorter time under visible light and is comparable with other photocatalysts.

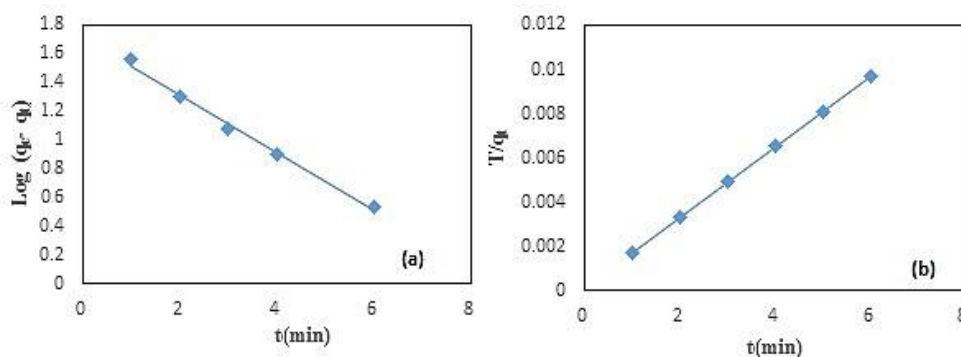


Fig. 8. Investigation of kinetic model of (a) first-pseudo and (b) second -pseudo.

Table 1. Comparison of proposed photocatalyst with other photocatalysts.

Photocatalyst	Concentration (ppm)	Photocatalyst Amount (g)	Time (min)	Ref
TiO ₂ /UV-C	15	0.12	56	[23]
TiO ₂	10	0.1	150	[24]
TiO ₂ /Alg/FeNPs	5	0.2	120	[25]
Ag-Al ₂ O ₃ .	100	0.1	120	[26]
Al-Sm M-hexaferrite	10	0.1	140	[27]
Fe ₃ O ₄ @SiO ₂ @CeO ₂	10	0.05	50	Present work

4. Conclusions

Improving the performance of photocatalysts is largely dependent on their particle size. The photocatalytic reaction rate increases dramatically by reducing the size of the particle and increasing the oxidation-reduction potential. The core-shell magnetic nanostructure has a large surface-to-volume ratio, which significantly increases its photocatalytic capacity. In this work, the use of the Fe₃O₄@SiO₂@CeO₂ nanostructure containing magnetic and semiconductor nanoparticles creates one of the most promising photocatalysts for dye pollutant removal. The presence of Fe₃O₄, due to its magnetic properties, makes the catalyst reusable. However, a direct contact of CeO₂, as the semiconductor, onto the surface of magnetic nanoparticles leads to unfavorable heterojunction. Because the small band gap of Fe₃O₄ can act as an electron-hole recombination center, it leads to lower photocatalytic activity. Thus, the SiO₂ layer between these two structures reduces the negative effects. The proposed core-shell photocatalyst in this research is appropriate for removing pollutants in the environment and destroying organic materials in water due to its photocatalytic properties, chemical stability, non-toxicity, and high activity under visible light radiation.

Acknowledgment

The authors would like to express their sincere appreciation to Mr. Alireza Afzalipour and his wife Mrs. Fakhreh Saba, the founders of the Shahid Bahonar University of Kerman, for their foresight and generosity in training the future generations of doctors, engineers, and scientists. Also, the authors would like to acknowledge Dr. Parviz Dabiri for his

support in the research activities of the chemistry and nano laboratories at the Shahid Bahonar University of Kerman.

References

- [1] Hitam, C. N. C., Jalil, A. A. (2020). A review on exploration of Fe₂O₃ photocatalyst towards degradation of dyes and organic contaminants. *Journal of environmental management*, 258, 110050.
- [2] You, J., Guo, Y., Guo, R., Liu, X. (2020). A review of visible light-active photocatalysts for water disinfection: Features and prospects. *Chemical engineering journal*, 373, 624-641.
- [3] Liang, Q., Liu, X., Zeng, G., Liu, Z., Tang, L., Shao, B., Zeng, Z., Zhang, W., Liu, Y., Cheng, M., Tang, W., & Gong, Sh. (2019). Surfactant-assisted synthesis of photocatalysts: Mechanism, synthesis, recent advances and environmental application. *Chemical engineering journal*, 372, 429-451.
- [4] Poole, Jr., Charles, P., Frank, J. (2005). Introduction to Nanotechnology. *Journal of materials science technology*, 395, 226-234.
- [5] Ohno, K., Tanaka, M., Takeda, J., Kawazoe, Y. (2008). Nano-and Micromaterials. *Materials letters*, 9, 123-136.
- [6] Wong, J. K. H., Tan, H. K., Lau, S. Y., Yap, P-S., Danquah, M. K. (2019). Potential and challenges of enzyme incorporated nanotechnology in dye wastewater treatment: A review. *Journal of environmental chemical engineering*, 7, 103261.
- [7] Kurmi, B. D., Patel, P., Paliwal, R., Paliwal, S. R. (2020). Molecular approaches for targeted drug delivery towards cancer: A concise review with respect to

- nanotechnology. *Journal of drug delivery science and technology*, 57, 101682.
- [8] Zhang, W., Zhang, D., Liang, Y. (2019). Nanotechnology in remediation of water contaminated by poly- and perfluoroalkyl substances: A review. *Environmental pollution*, 247, 266-276.
- [9] Hitkari, G., Singh, S., Panday, G. (2018). Photoluminescence behavior and visible light photocatalytic activity of ZnO, ZnO/ZnS and ZnO/ZnS/ α -Fe₂O₃ nanocomposites. *Transactions of nonferrous metals society of China*, 28, 1386-1396.
- [10] Qian, Y., Yang, M., Zhang, F., Du, J., Li, K., Lin, X., Zhu, X., Lu, Y., Wang, W., Kang, D. J. (2018). A stable and highly efficient visible-light-driven hydrogen evolution porous CdS/WO₃/TiO₂ photocatalysts. *Materials characterization*, 142, 43-49.
- [11] Ma, R., Zhang, S., Wen, T., Gu, P., Li, L., Zhao, G., Niu, F., Huang, Q., Tang, Zh., Wang, X. (2019). A critical review on visible-light-response CeO₂-based photocatalysts with enhanced photooxidation of organic pollutants. *Catalysis today*, 335, 20-30.
- [12] Chaudhuri, R. G., Paria, S. (2012). Core-shell nanoparticles: classes, properties, synthesis mechanisms, characterization, and applications. *Chemical reviews*, 112, 2373-2433.
- [13] Channei, D., Inceesungvorn, B., Wetchakun, N., & Phanichphant, S. (2014). Synthesis of Fe₃O₄/SiO₂/CeO₂ Core-Shell magnetic and their application as photocatalyst. *Journal of nanoparticle research*, 14, 7756-7762.
- [14] Girginova, P. I., Daniel-da-Silva, A. L., Lopes, C. B., Figueira, P., Otero, M., Amaral, V. S., Pereira, E., Trindade, T. (2010). Silica coated magnetite particles for magnetic removal of Hg²⁺ from water. *Journal of colloid and interface science*, 345, 234-240.
- [15] Panneerselvam, P., Morad, N., Tan, K. A. (2011). Magnetic nanoparticle (Fe₃O₄) impregnated onto tea waste for the removal of nickel (II) from aqueous solution. *Journal of imaging science and technology*, 186, 160-168.
- [16] Peng, Q., Liu, Y., Zeng, G., Xu, W., Yang, C., Zhang, J. (2010). Biosorption of copper (II) by immobilizing *Saccharomyces cerevisiae* on the surface of chitosan-coated magnetic nanoparticles from aqueous solution. *Journal of imaging science and technology*, 177, 676-682.
- [17] Tajabadi, M., Khosroshahi, M. E. (2012). New finding on magnetite particle size reduction by changing temperature and alkaline media concentration. *Advances in chemistry series*, 3, 140-146.
- [18] Mashkooor, F., Nasar, A. (2020). Magsorbents: Potential candidates in wastewater treatment technology – A review on the removal of methylene blue dye. *Journal of magnetism and magnetic materials*, 500, 166408.
- [19] Wang, C., Li, J., Lv, X., Zhang Y., Guo, G. (2014). Photocatalytic organic pollutants degradation in metal-organicframeworks. *Energy and environmental science*. 25, 2831-2867.
- [20] Zinatloo-Ajabshir, S., Salavati-Niasari, M. (2019). Preparation of magnetically retrievable CoFe₂O₄@SiO₂@Dy₂Ce₂O₇ nanocomposites as novel photocatalyst for highly efficient degradation of organic contaminants. *Composites part B: Engineering*, 174, 106930.
- [21] Long, Z., Li, Q., Wei, T., Zhang, G., Ren, Zh. (2020). Historical development and prospects of photocatalysts for pollutant removal in water. *Journal of hazardous materials*, 395, 122599.
- [22] Channei, D., Inceesungvorn, B., Wetchakun, N., Phanichphant, S. (2014). Synthesis of Fe₃O₄/SiO₂/CeO₂ Core-Shell Magnetic and Their Application as Photocatalyst. *Journal of nanoscience and nanotechnology*, 14, 7756-7762.
- [23] Ehrampoosh, M., Moussavi, G. H., Ghaneian, M., Rahimi, S., Ahmadian, M. (2011). Removal of methylene blue dye from textile simulated sample using tubular reactor and TiO₂/UV-C photocatalytic process. *Journal of environmental health*, 8, 34-40.
- [24] Joshi, K. M., Shrivastava, V. S. (2012). Removal of methylene blue dye aqueous solution using photocatalysis. *Environmental technology*, 2, 241-252.
- [25] Kanakaraju, D., Mohamad Shahdad, R. N., Lim, Y-C., Pace, A. (2018). Magnetic hybrid TiO₂/Alg/FeNPs triads for the efficient removal of methylene blue from water. *Sustainable chemistry and pharmacy*, 8, 50-62.
- [26] Saeed, M., Muneer, M., Akram, N., Haq, A., Afzal, N., Hamayun, M. (2019). Synthesis and characterization of silver loaded alumina and evaluation of its photocatalytic activity on photo degradation of methylene blue dye. *Chemical engineering research and design*, 148, 218- 226.
- [27] Ashraf, G. A., Rasool, R. T., Hassan, M., Zhang, L. (2020). Enhanced photo Fenton-like activity by effective and stable Al-Sm M-hexaferrite heterogenous catalyst magnetically detachable for methylene blue degradation. *Journal of alloys and compounds*, 821, 153410.